The high-pressure phase transition sequence from the rutile-type through to the cotunnite-type structure in $PbO_2$



1996 J. Phys.: Condens. Matter 8 1631

(http://iopscience.iop.org/0953-8984/8/11/009)

J. Phys.: Condens. Matter **8** (1996) 1631–1646. Printed in the UK

# The high-pressure phase transition sequence from the rutile-type through to the cotunnite-type structure in $PbO_2$

J Haines, J M Léger and O Schulte

CNRS, Laboratoire de Physico-Chimie des Matériaux, 1, Place A Briand, 92190 Meudon, France

Received 9 October 1995, in final form 2 January 1996

**Abstract.** Four phase transitions were observed in $PbO_2$ under pressure up to 47 GPa using x-ray diffraction in a diamond anvil cell. At close to 4 GPa, rutile-structured $PbO_2$ underwent a second-order transition to an orthorhombic, $CaCl_2$-type phase. Above 7 GPa, this $CaCl_2$-type phase transformed to a cubic phase with a $Pa\bar{3}$ modified fluorite structure. A transition to an orthorhombic phase was observed at 11.4 GPa. The intensities of the diffraction lines in this orthorhombic phase indicate a displacement of the lead ions from the fcc positions occupied in the cubic phase. This orthorhombic phase has similar cell constants ($a = 10.027(2)$ Å, $b = 5.246(1)$ Å, and $c = 5.116(1)$ Å at 26 GPa) to the orthorhombic I phase of $ZrO_2$ and also that of $HfO_2$, and could be isostructural. A further transition began above 29 GPa to a cotunnite-type phase, with space group $Pnam$, and $Z = 4$, and with $a = 5.443(18)$ Å, $b = 6.346(17)$ Å, and $c = 3.368(8)$ Å at 47 GPa. The coordination number of the lead ion is 6 in the first two phases, $6 + 2$ in phase III, most probably 7 in phase IV and 9 in phase V. The volume decreases observed in the three first-order transitions are 6.9, 1.4, and 7.5% at 7, 11.4, and 29 GPa, respectively. The two higher-pressure transitions were reversible, whereas the cubic phase transformed to $\alpha$-$PbO_2$ upon decompression, and this was retained down to ambient pressure. This is the first time a cotunnite-type structure has been adopted by a group IVb dioxide, which has implications for the high-pressure behaviour of the homologous compounds with smaller cations: $SiO_2$, $GeO_2$ and $SnO_2$.

## 1. Introduction

$PbO_2$ is the rutile-type dioxide with the largest cation and can therefore be expected to be suitable as a model for the other rutile-type dioxides; radius ratio criteria indicate that $PbO_2$ should undergo the same transitions as the others, but at lower pressures. Tetragonal, rutile-type $\beta$-$PbO_2$ (phase I) transforms to orthorhombic $\alpha$-$PbO_2$ (phase II) above 1.3 GPa and 200 °C [1]. Quenching experiments indicated a transition to phase III, for which a cubic, fluorite-type structure was proposed, above 6 GPa at temperatures between 300 and 600 °C with a positive $P$–$T$ slope [2]. An *in situ* high-temperature, high-pressure x-ray diffraction study, using a cubic-anvil-type apparatus, however, indicated that the phase boundary has, in fact, a negative slope with an ambient-temperature transition pressure of 6.9 GPa [3]. Using an ungasketed diamond anvil cell (dac), $PbO_2$ was investigated up to 24 GPa with laser heating. In this study, the compound was reported to transform first to $\alpha$-$PbO_2$, then to a tetragonal fluorite-type phase at 9 GPa, and subsequently to the fluorite-type phase above 18 GPa [4]. Another study, for pressures up to 33 GPa, using a gasketed dac with resistive heating, indicated that on the contrary the fluorite-type phase is obtained at lower pressures than the tetragonal phase, which was labelled phase IV [5]. We have shown recently that

0953-8984/96/111631+16$19.50  

all of the cubic high-pressure phases of the rutile-type dioxides, including $PbO_2$, have a $Pa\bar{3}$ modified fluorite structure instead of a fluorite structure [6].

The orthorhombic cotunnite ($PbCl_2$) structure, in which the cation is in ninefold coordination, has been proposed for the high-pressure phases of several metal dioxides, $ZrO_2$, $HfO_2$, $UO_2$, $TbO_2$, $CeO_2$, $ThO_2$, $PuO_2$, and $TeO_2$, based on cell constants or Raman spectra [7–13]. The structure of cotunnite-type $ZrO_2$ has been refined using x-ray powder diffraction data from a quenched sample at ambient pressure and *in situ* at high pressure [14]. Up to the present, $PbO_2$ has not been found to adopt this structure, although $Pb^{4+}$ is larger than $Zr^{4+}$, $Hf^{4+}$ and $Te^{4+}$. The present study was undertaken in order to discover whether $PbO_2$ adopts the cotunnite structure at pressures higher than those obtained in previous studies and to investigate the 'fluorite-type' and 'tetragonal' high-pressure phases in detail.

## 2. Experimental procedure

Powdered $PbO_2$ (Alfa Products) was mixed with silicone grease as the pressure-transmitting medium and was placed in 150–200 $\mu$m diameter holes of stainless-steel gaskets, preindented to a thickness of 120 $\mu$m, along with a very small amount of ruby powder between the anvils of a diamond anvil cell. Pressures were measured on the basis of the shift of the ruby $R_1$ and $R_2$ fluorescence lines [15]. X-ray diffraction patterns were obtained on film placed cylindrically at a radius of 25.10 mm using zirconium-filtered molybdenum radiation from a fine-focus tube collimated to 130 $\mu$m. A second experiment was performed up to 30 GPa using an imaging plate placed at distances between 84.85 and 147.90 mm from the sample. Exposure times were of the order of 24–48 hours and all of the experiments were performed at room temperature. The observed intensities on the films and imaging plate were integrated as a function of $2\theta$ to yield one-dimensional diffraction patterns. The instrumental resolution, as limited by the spatial resolution of the microdensitometer and the image plate reader, was $0.1^\circ$ in $2\theta$ for the film data and $0.02$–$0.03^\circ$ for the imaging plate data depending on the sample-to-plate distance. There are additional contributions due, in particular, to the sample, and for $\beta$-$PbO_2$, full width at half-maximum values were of the order of $0.35^\circ$ for the film data and $0.25^\circ$ for the image plate data. A standard diffractometer scan was performed prior to the experiment and Debye–Scherrer photographs were obtained for the materials recovered after the experiment using Cu radiation. The observed peaks from the film data were fitted to gaussians, and the resulting positions were used for unit cell refinement. The image plate data were analysed by profile refinement. Residual K$\beta$ reflections at 4% intensity with respect to the K$\alpha$ reflections were also fitted in the profile refinement such that peaks partially overlapped by K$\beta$ lines could still be measured with precision. Simulations and profile refinements were performed using the program Fullprof [16]. All figures in parentheses refer to standard deviations.

## 3. Results and discussion

### *3.1. Phases I and I′*

The starting material was found be exclusively rutile structured ($P4_2/mnm$, $Z = 2$) with the following cell constants: $a = 4.9532(5)$ Å and $c = 3.3854(5)$ Å. At close to 4 GPa, the reflections $hkl$, $h \neq k$, were found to broaden and then subsequently split with further increases in pressure. This is typical of an orthorhombic distortion of the tetragonal phase. There are no discontinuities in the cell constants and the relative volume (see figures 1 and 2),

**Table 1.** High-pressure diffraction data ($I/I_{100} > 3\%$) for $CaCl_2$-type $PbO_2$, phase I′; $a = 4.930(2)$ Å, $b = 4.814(2)$ Å, $c = 3.363(1)$ Å, space group *Pnnm*, $Z = 2$, at 7.3 GPa.

| $d$ (Å) | $I_{obs}$ | $I_{calc}$ [a] | $hkl$ |
|---|---|---|---|
| 3.444 | 100 | 100 | 110 |
| 2.778 | 43 | 43 | 101 |
| 2.757 | 43 | 45 | 011 |
| 2.465 | 20 | 22 | 200 |
| 2.407 | 9 | 11 | 020 |
| 1.838 | 29 | 36 | 211 |
| 1.819 | 29 | 34 | 121 |
| 1.722 | 14 | 16 | 220 |
| 1.682 | 6 | 7 | 002 |
| 1.555 | 11 | 12 | 310 |
| 1.526 | 9 | 8 | 130 |
| 1.511 | 17 | 16 | 112 |
| 1.476 | 12 | 12 | 301 |
| 1.448 | 6 | 7 | 031 |
| 1.389 | 5 | 5 | 202 |
| 1.379 | 4 | 4 | 022 |
| 1.259 | 7 | 7 | 321 |
| 1.249 | 6 | 8 | 231 |
| 1.203 | 8 | 7 | 222 |
| 1.148 | 3 | 3 | 330 |
| 1.142 | 6 | 6 | 312 |
| 1.130 | 6 | 5 | 132 |
| 1.125 | 6 | 6 | 411 |
| 1.104 | 5 | 4 | 141 |
| 1.097 | 3 | 3 | 420 |

[a] Calculated using Fullprof with $Pb^{4+}$ on 2a sites (0, 0, 0) and $O^{2-}$ on 4g sites (0.338, 0.261, 0.000) (fixed); the scale factor, lineshape parameters, overall thermal parameter, strain and preferred orientation parameters and cell constants were varied in the profile refinement.

indicating that this transition is continuous. Second-order transitions from the tetragonal rutile-type structure to the orthorhombic $CaCl_2$-type structure ($Pnnm, Z = 2$) have been observed for a series of dioxides: $SiO_2$ [17, 18], $MnO_2$ [19], $RuO_2$ [20] and $SnO_2$ [21], and the present diffraction data are in good agreement with this structure; see table 1. In the present case, the $CaCl_2$-type phase appears to be strictly metastable, appearing in the pressure range of stability of $\alpha$-$PbO_2$ [1], and hence we label it phase I′.

### *3.2. Phase III*

The transition to phase III was found to begin immediately above 7 GPa with a $\Delta V$ of 6.9(1)% (figures 1 and 2). The positions of the observed diffraction lines of this phase are in agreement with a cubic cell and no broadening of the lines expected to split if a tetragonal distortion was present was observed. The present results are in agreement with those of Yagi and Akimoto [3] and those of Ming and Manghnani [5] in that the phase obtained at this pressure is in fact cubic. In the former study, the 12 diffraction lines observed were all in very good agreement with a cubic cell.

Up to the present, it has been assumed that cubic $PbO_2$ has the fluorite structure. We have shown, however, that the structures of all of the cubic high-pressure phases of the dioxides which are rutile-structured under ambient conditions are of the $Pa\bar{3}$ modified

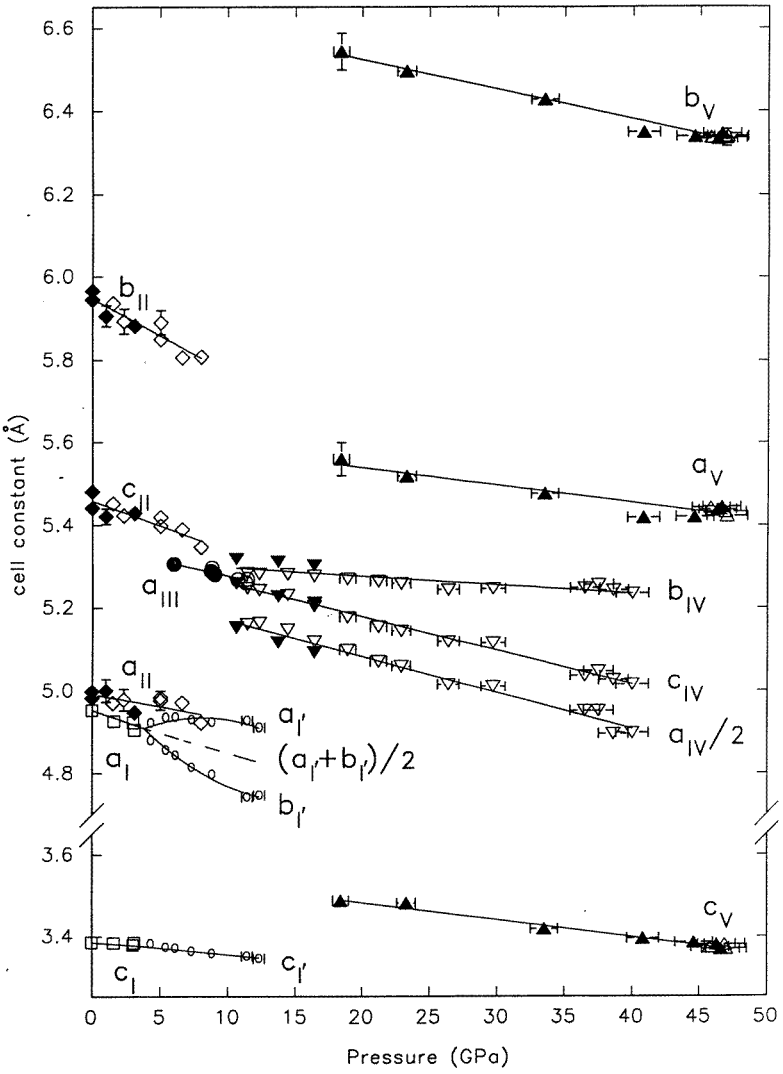


**Figure 1.** Cell constants of $PbO_2$ as a function of pressure. Open symbols refer to points obtained upon compression and solid symbols to those obtained on decompression. Symbols □, o, ◊, ○, ▽ and △ correspond to phases I, I′, II, III, IV and V, respectively. Solid lines represent a linear or a quadratic least-squares fit of the data for each phase. Error bars are shown where the error is larger than the symbol size. Open diamonds (◊) correspond to phase II points obtained on the second compression run only.

fluorite type [6]. Cubic $PbO_2$ is no exception and Rietveld refinement of the structure at 9.0 GPa yielded $a = 5.2804(3)$ Å and the oxygen coordinate $u = 0.332(2)$ ($R_{Bragg} = 4.0\%$, $R_p = 11.0\%$, $R_{wp} = 8.3\%$) [6]. In this structure, the lead ion is in $6 + 2$ coordination with six anions at 2.156 Å and two at 3.033 Å forming a regular rhombohedron; the shortest O–O distance is 2.777 Å. In a fluorite structure ($u = 0.25$) with the same volume, the eight polyhedral Pb–O distances and the shortest O–O distance would be 2.2865 and 2.6402 Å, respectively.

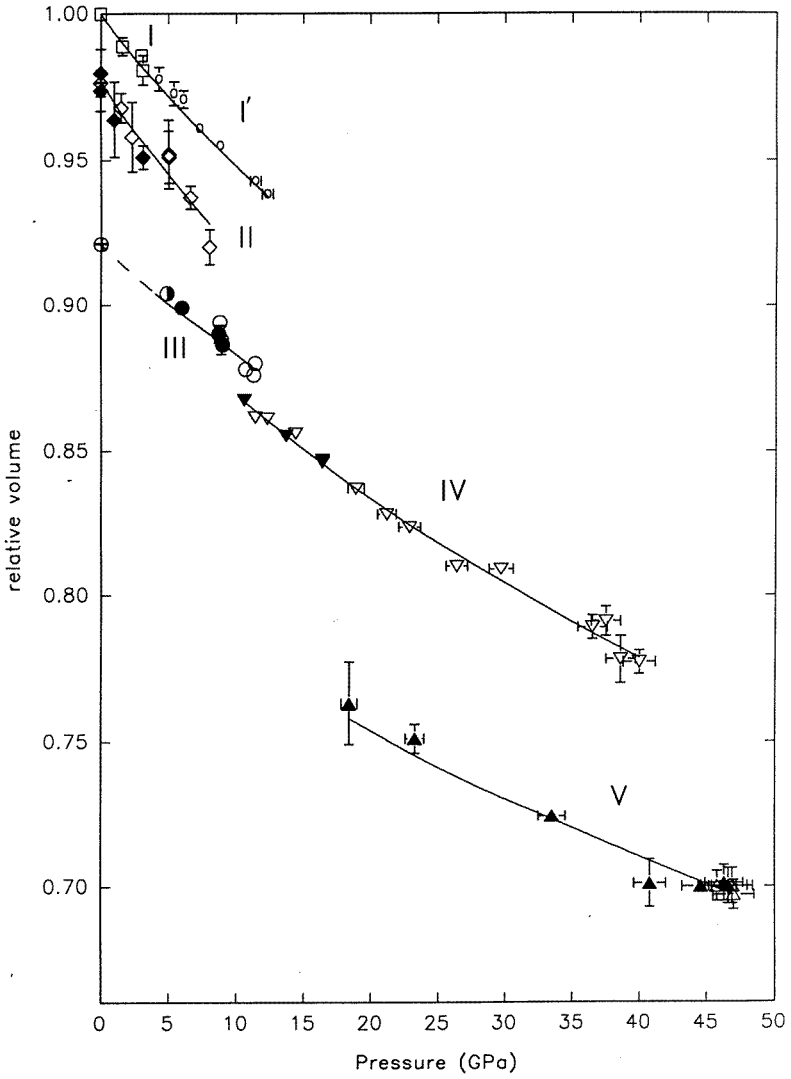


**Figure 2.** The relative volume of $PbO_2$ as a function of pressure. The key is as for figure 2. The points shown as the crossed diamond and the crossed open circle are from [2] and the half-filled circle is from [3]. Solid lines represent Birch–Murnaghan equations of state using the parameters listed in table 5.

The phase I–phase III transition did not proceed via phase II ($\alpha$-$PbO_2$, $Pbcn$, $Z = 4$), but rather via the metastable $CaCl_2$-type phase I′. A $CaCl_2$-type phase was observed as a stable intermediate between the rutile and cubic phases of $RuO_2$ [20]. The rutile $\rightarrow$ $CaCl_2$ $\rightarrow$ $Pa\bar{3}$ transition sequence can occur via a diffusionless process involving a displacement of the oxygen ions. In contrast, the transition from the rutile phase to $\alpha$-$PbO_2$ requires changes to both the $Pb^{4+}$ and $O^{2-}$ sublattices and appears to need thermal activation or high shear stresses, as in the case of the ungasketed dac experiment [4]. Similar behaviour is observed for $TiO_2$ and $SnO_2$. If rutile [22] is heated at pressures above 5 GPa, an $\alpha$-$PbO_2$-type phase is obtained; however, at room temperature, rutile transforms directly to a higher-

**Table 2.** Results from the partial structure refinement of $PbO_2$ phase IV; $a = 10.023(2)$ Å, $b = 5.246(1)$ Å, $c = 5.116(1)$ Å, space group *Pbca*, $Z = 8$, at 26.4 GPa. All of the ions are on 8c sites: $Pb^{4+}$: (0.8861(3), 0.0250(4), 0.2638(10)); $O^{2-}(1)$: (0.7963, 0.3800, 0.1381) (fixed); $O^{2-}(2)$: (0.9777, 0.7500, 0.4901) (fixed). Agreement factors: $R_{Bragg} = 3.7\%$, $R_p = 8.0\%$, $R_{wp} = 6.4\%$.

| $d$ (Å) | $I_{obs}$ | $I_{calc}$ | $hkl$ |
|---|---|---|---|
| 3.624 | 3 | 3 | 210 |
| 3.440 | 2 | 1 | 111 |
| 2.957 | 100 | 100 | 211 |
| 2.623 | 28 | 28 | 020 |
| 2.558 | 12 | 12 | 002 |
| 2.507 | 10 | 10 | 400 |
| 2.334 | 3 | 2 | 021 |
| 2.090 | 1 | 1 | 212 |
| 2.069 | 3 | 3 | 411 |
| 1.831 | 14 | 13 | 022 |
| 1.812 | 12 | 11 | 420 |
| 1.790 | 9 | 8 | 402 |
| 1.708 | 2 | 2 | 421 |
| 1.651 | 3 | 3 | 230 |
| 1.571 | 14 | 14 | 231 |
| 1.543 | 9 | 8 | 213 |
| 1.520 | 8 | 7 | 611 |
| 1.479 | 6 | 6 | 422 |
| 1.387 | 2 | 2 | 232 |
| 1.311 | 1 | 1 | 040 |
| 1.270 | 1 | 1 | 041 |
| 1.186 | 2 | 2 | 233 |
| 1.175 | 2 | 2 | 631 |
| 1.164 | 2 | 1 | 613 |

pressure phase, baddeleyite, above 12 GPa. In the case of $SnO_2$ [21, 23], the high-pressure transition from the rutile-type to the $\alpha$-$PbO_2$-type phase is observed upon heating. At room temperature, however, only a small amount of the $\alpha$-$PbO_2$-type phase is formed and the vast majority of the $SnO_2$ undergoes the sequence of transitions observed for $RuO_2$ and $PbO_2$.

### *3.3. Phase IV*

Above 11.4 GPa, the cubic 200, 220 and 311 reflections were found to broaden and no longer gave the same cell constant. In addition many new weak reflections—see table 2—were observed, which are absent for a fcc cell. The appearance of these new reflections indicates that the lead ions are displaced from the fcc positions occupied in phase III. In the $Pa\bar{3}$ phase, the few, very weak, non-fcc reflections arise uniquely from the anion sublattice and all have values of $I/I_{100}$ of less than 1%. These changes to the diffraction pattern are consistent with a distortion of the parent $Pa\bar{3}$-structured phase. The two previous investigations of this phase both concluded that it had tetragonal symmetry [4, 5] and it was proposed that it could have a structure related to those of the high-temperature tetragonal phases of $ZrO_2$ and $HfO_2$ [24, 25]. It is evident from the present study that it is in fact orthorhombic—see table 2. It should be noted that the 'tetragonal' high-pressure phases of $ZrO_2$, $HfO_2$ and $MnF_2$ have also all been shown to be orthorhombic [26–28]. The volume

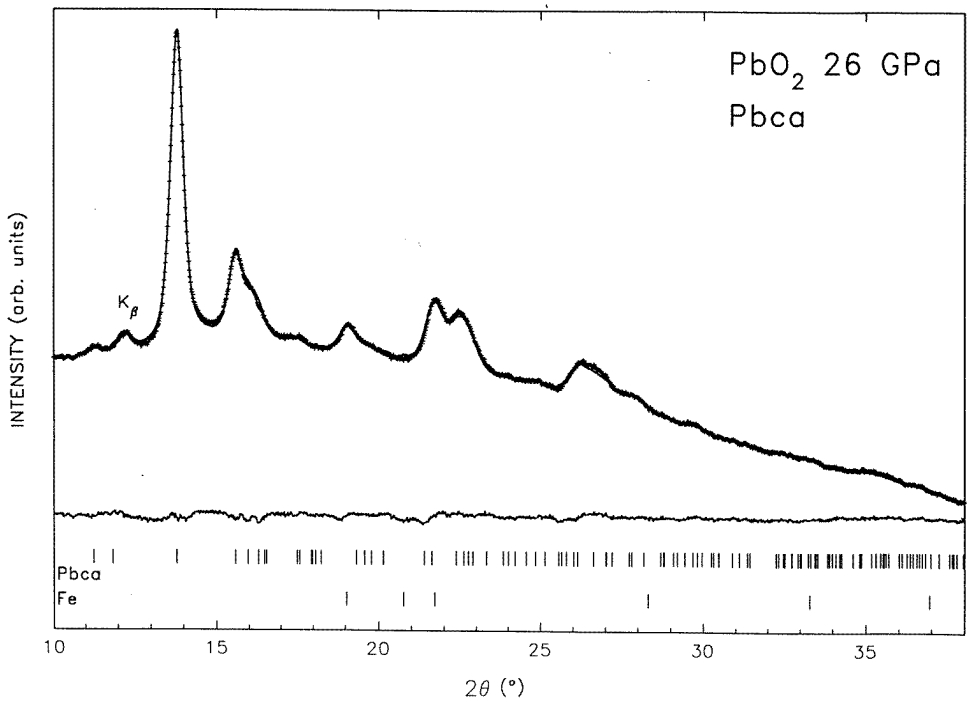


**Figure 3.** The experimental profile from image plate data (+) and the calculated profile (solid line) from partial structure refinement of orthorhombic $PbO_2$ phase IV at 26.0 GPa using a *Pbca* structural model. The intensity is in arbitrary units and the difference profile is on the same scale. Vertical bars indicate the calculated positions of diffraction peaks (K$\alpha$) of the *Pbca* model and iron from the gasket ($\varepsilon$-Fe). K$\beta$ indicates the most intense K$\beta$ reflection ($I/I_{100} = 4\%$). Agreement factors: $R_{Bragg} = 3.7\%$, $R_p = 8.0\%$, $R_{wp} = 6.4\%$ ($p$ = profile, $wp$ = weighted profile).

change between the cubic and orthorhombic phases of $PbO_2$ is 1.4(1)% at 11.4 GPa.

Structural models based on orthorhombic distortions of tetragonal $ZrO_2$, $HfO_2$ and the proposed high-pressure structure [29] of 'tetragonal' $MnF_2$ were not retained, as the non-fcc reflections for these structures originate from a displacement of the anions from fluorite-type positions and, in fact, calculations give essentially zero intensity for these reflections. An orthorhombic structure with the space group $Aba2$ has been proposed for $MnF_2$ based on theoretical calculations [30]. A good fit can be obtained for the fcc reflections with this model; however, the agreement for the remaining reflections is poor. It should be noted that in this structure model the lead ions are only free to move along $z$. Attention was then concentrated on the highest-symmetry subgroups of $Pa\bar{3}$, in which all three lead coordinates were free, $P2_12_12_1$ and $Pbc2_1$, the latter being a subgroup of $Aba2$. Partial structure refinements were performed starting from the positions adopted in the cubic phase. The oxygen positions were not varied as their effect on the profile was not significant enough to permit a stable minimum to be obtained. $R_{Bragg}$-factors of 4–5% were obtained for both models with displacements of the lead ions of up to 0.05 along a given direction from fcc positions with the better overall fit being obtained for the $Pbc2_1$ model. It was noted, however, that for both models a reflection ($I/I_{100} = 2\%$) was missing in the calculated pattern on the low-angle side of the 111 K$\beta$ reflection. This is where the 111 reflection

**Table 3.** Mean linear compressibilities ($10^{-4}$ GPa$^{-1}$) and ambient cell constants (Å) for $PbO_2$.

| Phase | $K_a$ | $K_b$ | $K_c$ | $a_0$ | $b_0$ | $c_0$ |
|---|---|---|---|---|---|---|
| I | 23(1) | — | 7(1) | 4.9532(5) | — | 3.3854(5) |
| III | 13.6(4) | — | — | 5.3492[a] | — | — |
| IV | 17(1) | 4(1)[b] | 15(1) | 10.512(18) | 5.318(8) | 5.340(5) |
| V | 8(1) | 11(1) | 12(1) | 5.622(16) | 6.665(11) | 3.566(16) |
| II | 12(4) | 30(3) | 22(4) | 4.991(9) | 5.948(9) | 5.458(9) |

[a] $a_0$ from Syono and Akimoto [2].

[b] Data on decompression give $K_b = 8 \times 10^{-4}$ GPa$^{-1}$ with $b_0 = 5.370$ Å. Note: the cell constants in phase I′ were fitted to the following polynomials:

$$a = 4.909 + 1.29 \times 10^{-3}(p - 3.8) - 1.4 \times 10^{-3}(p - 3.8)^2$$
$$b = 4.909 - 3.18 \times 10^{-2}(p - 3.8) + 1.44 \times 10^{-3}(p - 3.8)^2$$
$$c = 3.376 - 3.35 \times 10^{-3}(p - 3.8).$$

of a $2a$ supercell could be expected, and which is observed for the orthorhombic high-pressure phases of $ZrO_2$ and $HfO_2$ that do in fact have a doubled cell along $a$ and are the only known examples of a $Z = 8$ fluorite-derived cell at high pressure in the dioxides. The cell constants of the orthorhombic phase, phase I, of $ZrO_2$ under ambient conditions are $a = 10.0861$ Å, $b = 5.2615$ Å, and $c = 5.0910$ Å [26], which can be compared to $a = 10.027(2)$ Å, $b = 5.246(1)$ Å, and $c = 5.116(1)$ Å for $PbO_2$ at 26 GPa. In addition, in both compounds the compression is very anisotropic. In $PbO_2$ (see table 3) $\boldsymbol{b}$ is significantly less compressible than $\boldsymbol{a}$ or $\boldsymbol{c}$ as is the case for $ZrO_2$ [26, 31]. Due to the similarities between the cell constants and the linear compressibilities of $PbO_2$ phase IV and orthorhombic I phase $ZrO_2$, a partial structure refinement with an orthorhombic I phase structural model, $Pbca$, $Z = 8$, was performed. This refinement yielded a very good fit ($R_{Bragg} = 3.7\%$) to the experimental profile—see figure 3—with displacements of the lead ions of less than 0.025 from fcc positions—see table 2. This would result in the lead ion having a coordination number (CN) of 7. This structure will have to be confirmed as there are many other possible arrangements for the oxygen sublattice, all of which result in only very slight modifications to the calculated x-ray diffraction profile. It is therefore necessary to obtain neutron diffraction data for this phase in order to refine the structure.

The data of Liu for the 'tetragonal' phase observed after laser heating at 24 GPa [4] agree well with the summits of peak clusters in the present study; the differences are primarily due to the lower resolution and lower sensitivity available at that time. In this previous study, prior to laser heating, the four diffraction lines observed were attributed to phase III; however, the 200, 220 and 311 reflections were broad, indicating an unresolved splitting of these lines and hence the presence of the orthorhombic distortion revealed here. The data of Ming and Manghnani [5], obtained both *in situ* at between 540 and 600 °C and after heating, are in agreement with ours in so far as the sequence of phases is concerned. The transition from phase III to phase IV was observed at above 23 GPa, which was probably due to the difficulty in detecting the structural distortion at lower pressures given the limited resolution available. The relative volumes reported by these authors for phase IV are 8% higher than both the present data and the data of Liu [4].

### *3.4. Phase V*

Above 29 GPa, new reflections were observed, which increased in intensity at the expense of those of phase IV with further compression up to 47 GPa, the highest pressure reached.

The kinetics of this transition are slow and a significant proportion of phase IV remained at 47 GPa. A large pressure range of hysteresis was observed with the reverse transition beginning below 20 GPa, and a small amount of this new phase appeared to be retained down to ambient pressure.

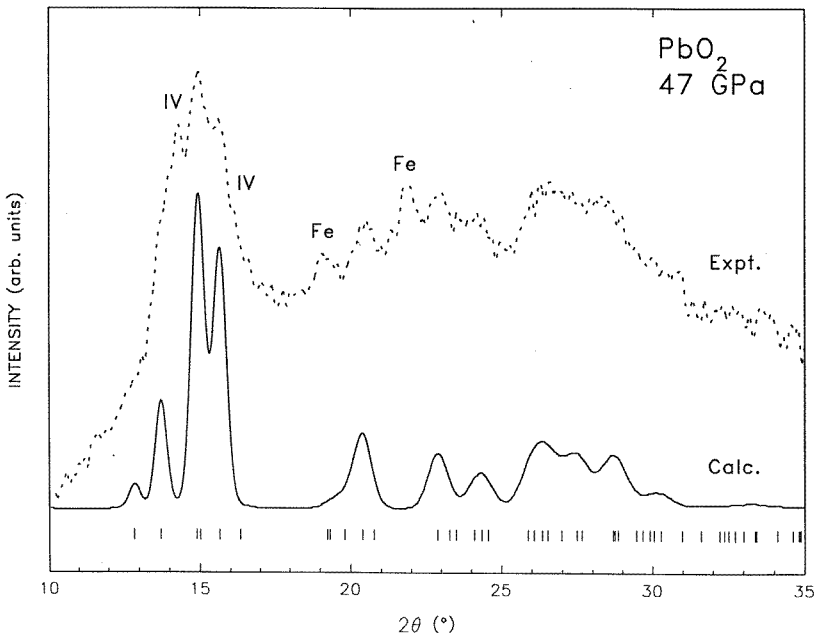


**Figure 4.** The experimental profile (dashed line) of $PbO_2$ phase V at 47 GPa obtained from film data and the calculated profile (solid line) based on a cotunnite-type structure with the cell constants and atomic positions given in table 4. The intensity is in arbitrary units. Vertical bars indicate the calculated positions of diffraction peaks for the cotunnite-type structure. Diffraction peaks remaining from phase IV and iron from the gasket are labelled IV and Fe, respectively.

The diffraction pattern of this new phase, phase V, could be indexed based on an orthorhombic, cotunnite-type cell, and the observed intensities are in good agreement with a cotunnite-type structure ($Pnam$, $Z = 4$) with atomic positions similar to those of cotunnite-type $ZrO_2$ [14] and $PbCl_2$ [32] (table 4 and figure 4). This transition represents an increase in coordination number of the lead ions to 9, with the anions forming elongated tricapped trigonal prisms containing the cations. The observed volume decrease on going from phase IV to phase V is 7.5(3)% at 29 GPa, which is in good agreement with the volume decrease of 7.5% at 31.5 GPa observed for the fluorite-to-cotunnite transition in $CeO_2$ [11]. In addition, the difference in initial relative volumes of phases IV and V, 10(1)%, see table 5, is in agreement with the differences observed between the orthorhombic I and orthorhombic II phases of $ZrO_2$ and $HfO_2$ [7, 14, 26, 27].

The lattice parameters of phase V can be related to those of phase IV as follows: $\boldsymbol{a}_V = \boldsymbol{b}_{IV}, \boldsymbol{b}_V = \frac{1}{2}\boldsymbol{a}_{IV} + \boldsymbol{c}_{IV}$ and $\boldsymbol{c}_V = \frac{1}{2}(\boldsymbol{c}_{IV} - \frac{1}{2}\boldsymbol{a}_{IV})$; see table 6. Such a transformation would, however, require significant modification to both the cationic and anionic sublattices, as in the cotunnite structure all of the atoms lie in planes at $z = 1/4$ and $z = 3/4$.

The axial ratios $a/c$ and $b/c$ of cotunnite-type $PbO_2$ at 47 GPa are 1.616(9) and 1.884(9), respectively. These values lie well within the range of values observed for cotunnite-

**Table 4.** High-pressure diffraction data for cotunnite-type $PbO_2$, phase V; $a = 5.443(18)$ Å, $b = 6.346(17)$ Å, $c = 3.368(8)$ Å, at 47 GPa, space group *Pnam*, $Z = 4$. Calculated intensities obtained with all ions on 4c sites: $Pb^{4+}$: (0.260, 0.100, 0.250); $O^{2-}(1)$: (0.360, 0.430, 0.250); $O^{2-}(2)$: (0.020, 0.340, 0.750). IV = phase IV reflection.

| $d_{obs}$ (Å) | $d_{calc}$ (Å) | $I_{obs}$ | $I_{cal}$ | $hkl$ |
|---|---|---|---|---|
| 3.177 | 3.173 | 6 | 6 | 020 |
| 2.981 | 2.975 | 39 | 30 | 011 |
| 2.877 | | 73 | | IV |
| 2.739 | 2.741 | 100 | 65 | 120 |
| | 2.721 | | 35 | 200 |
| 2.621 | 2.611 | 79 | 84 | 111 |
| 2.520 | | 19 | | IV |
| 1.998 | 2.008 | 30 | 32 | 211 |
| 1.790 | 1.791 | 38 | 28 | 031 |
| 1.684 | 1.684 | 14 | 14 | 002 |
| 1.567 | 1.575 | 17 | 17 | 320 |
| 1.544 | 1.549 | 21 | 23 | 311 |
| 1.494 | 1.496 | 29 | 28 | 231 |
| 1.437 | 1.435 | 37 | 22 | 122 |
| | 1.432 | | 12 | 202 |
| 1.365 | 1.371 | 18 | 6 | 240 |
| | 1.361 | | 5 | 400 |

**Table 5.** Equation of state parameters for $PbO_2$. Note: values with no standard deviation were fixed, except $B_0'$ for H11 which was calculated.

| | Birch–Murnaghan | | | H11 | | |
|---|---|---|---|---|---|---|
| Phase | $B_0$ (GPa) | $B_0'$ | $V_0$ | $B_0$ (GPa) | $B_0'$ | $V_0$ |
| I | 176(16) | 4 | 1.000 | 175(13) | 3.7 | 1.000 |
| I′ | 167(18) | 4 | 1.001 | 170(14) | 3.8 | 1.001 |
| III | 223(7) | 4 | 0.921[a] | 223(7) | 3.7 | 0.921[a] |
| IV | 180(7) | 4 | 0.915(3) | 181(7) | 3.8 | 0.914(3) |
| V | 221(21) | 4 | 0.815 | 225(17) | 3.8 | 0.815 |
| II | 141(10) | 4 | 0.978[b] | 141(12) | 3.9 | 0.978[b] |

[a] $V_0$ for phase III was from Syono and Akimoto [2].
[b] $V_0$ for phase II was from Syono and Akimoto [2].

structured compounds and are close to those of cotunnite-type $CeO_2$, $ThO_2$ and $PuO_2$: 1.605–1.634 and 1.882–1.897, respectively [11, 12]. There appear to be two distinct types of cotunnite-type oxide based on axial ratios: those oxides with the smaller cations, $ZrO_2$ [14] and $HfO_2$ [7], with values of $(a/c, b/c)$ of (1.678, 1.945) and (1.676, 1.951) respectively, and the above-mentioned compounds with larger cations.

Beck [33] has classified compounds with the cotunnite (CN = 9) and related $Co_2Si$ (CN = 10) structures as a function of $a/b$ and $(a + b)/c$; characteristic axial ratios are observed for the various different classes of $AX_2$ compounds such as the halides, sulphides and hydrides among others. At the time, there were no examples of cotunnite-structured oxides. If we combine the present results for $PbO_2$ with those for the other cotunnite-type oxides, it becomes evident that these oxides also have characteristic axial ratios lying within the following ranges: $a/b = 0.836$–$0.866$ and $(a + b)/c = 3.50$–$3.63$. These ranges

are close to those of the cotunnite-structured compounds with small anions such as the hydrides, fluorides and phosphides, and $Co_2P$, and are significantly different from those for the cotunnite-structured compounds containing large anions such as the remaining halides and chalcogenides.

We have recently found that $SnCl_2$, $PbCl_2$ and $BaX_2$ (X = Cl, Br, I) transform to a postcotunnite structure [34–36] related to that of $Co_2Si$, in which the coordination number is 10, and that $BaF_2$ adopts the $Ni_2In$-type structure (CN = 11) at high pressure [37]. In the cotunnite-type phases of these compounds, the $\boldsymbol{a}$-direction is highly compressible, and as a result the representative points for these compounds on the Beck plot shift towards those of their respective high-pressure phases with increasing pressure. This is not the case for cotunnite-type $ZrO_2$ [14] and $PbO_2$ for which the representative points shift only slightly, and actually move away from those of these potential high-pressure phases due to the greater compressibility along $\boldsymbol{c}$ in these phases. It is thus not possible to predict the next step in the phase transition sequence of the dioxides.

It was noted [11] that for the cotunnite-type oxides the transition pressures did not decrease with increasing cation radius as had been expected on the basis of radius ratio criteria. $ZrO_2$ and $HfO_2$ begin to transform if heated to 1000 °C at 10 and 16 GPa [7], respectively, and $ZrO_2$ has been observed to transform at 16 GPa at ambient temperature [38]. In contrast, the oxides with larger cations ($UO_2$, $TbO_2$, $CeO_2$, $ThO_2$ and $PuO_2$) all transform to the cotunnite structure at above 29 GPa at ambient temperature [8–12]. An explanation for this can be obtained from the results of *ab initio* calculations for $ZrO_2$ [57], which indicate that the cotunnite-type structure is more stable than the lower-pressure monoclinic and orthorhombic structures at all pressures. These lower transition pressures could therefore be due to the relative instability of the lower-pressure orthorhombic and monoclinic phases in $ZrO_2$ and $HfO_2$.

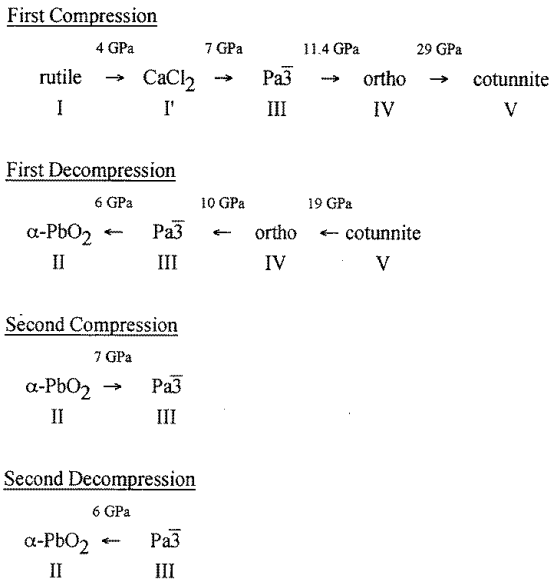


**Figure 5.** The sequence of phase transitions and transition pressures observed for $PbO_2$ in the present study. It must be noted that for most of these transitions there are large pressure ranges of two-phase intergrowth.

### *3.5. Decompression and the formation of phase II*

The reverse transitions from phase V to phase IV and then subsequently to phase III were observed; see figure 5. In both cases, hysteresis was observed, which was much more marked for the reconstructive V $\rightarrow$ IV transition. In agreement with previous investigations [1, 3, 4], phase III was found to transform to orthorhombic $\alpha$-$PbO_2$ (phase II), which was retained to ambient pressure. $\alpha$-$PbO_2$ was also recovered from shock wave experiments [39]. The cell constants obtained in the present study for $\alpha$-$PbO_2$ at ambient pressure are $a = 4.998(18)$ Å, $b = 5.945(18)$ Å, and $c = 5.481(12)$ Å.

**Table 6.** Structural data for the phases of $PbO_2$. Note: values without standard deviations are either fixed by symmetry or are fixed to reasonable values on the basis of the literature.

| Phase | Space group | $P$ (GPa) | Cell constants (Å) | Site | Positions |
|---|---|---|---|---|---|
| I[a] | $P4_2/mnm$, $Z = 2$ | 0.0001 | $a = 4.9556(1)$ | $Pb^{4+}$ 2a | 0, 0, 0 |
| | rutile-type | | $c = 3.3867(1)$ | $O^{2-}$ 4f | 0.3066(2), 0.3066(2), 0 |
| I′ | $Pnnm$, $Z = 2$ | 7.3 | $a = 4.930(2)$ | $Pb^{4+}$ 2a | 0, 0, 0 |
| | $CaCl_2$-type | | $b = 4.814(2)$ | $O^{2-}$ 4g | 0.338, 0.261, 0 |
| | | | $c = 3.363(1)$ | | |
| III | $Pa\bar{3}$, $Z = 4$ | 9.0 | $a = 5.2804(3)$ | $Pb^{4+}$ 4a | 0, 0, 0 |
| | modified fluorite-type | | | $O^{2-}$ 8c | 0.332(2), 0.332(2), 0.332(2) |
| IV | $Pbca$, $Z = 8$ | 26.4 | $a = 10.023(2)$ | $Pb^{4+}$ 8c | 0.8861(3), 0.0250(4), 0.2638(10) |
| | orthorhombic I phase | | $b = 5.246(1)$ | $O^{2-}$(1) 8c | 0.7963, 0.3800, 0.1381 |
| | $ZrO_2$-type | | $c = 5.116(1)$ | $O^{2-}$(2) 8c | 0.9777, 0.7500, 0.4901 |
| | model structure | | | | |
| V | $Pnam$, $Z = 4$ | 47 | $a = 5.443(18)$ | $Pb^{4+}$ 4c | 0.260, 0.100, 0.250 |
| | cotunnite-type | | $b = 6.346(17)$ | $O^{2-}$(1) 4c | 0.360, 0.430, 0.250 |
| | | | $c = 3.368(8)$ | $O^{2-}$(2) 4c | 0.020, 0.340, 0.750 |
| II[a] | $Pbcn$, $Z = 4$ | 0.0001 | $a = 4.9898(3)$ | $Pb^{4+}$ 4c | 0, 0.1779(7), 0.250 |
| | $\alpha$-$PbO_2$ | | $b = 5.9474(4)$ | $O^{2-}$ 8d | 0.2685(10), 0.4010(7), 0.4248(7) |
| | | | $c = 5.4656(3)$ | | |

[a] Data from Hill [40].

In order to calculate the bulk modulus for $\alpha$-$PbO_2$, additional data were obtained on recompression. This phase began to transform to phase III at 7 GPa with a volume decrease of 4%. Complete transformation to phase III was achieved at 11.3 GPa. Upon decompression, the reverse transition was observed; however, the cell constants obtained at ambient pressure were slightly different: $a = 4.982(13)$ Å, $b = 5.966(14)$ Å and $c = 5.441(11)$ Å. It has been noted that variations in cell constants of $\alpha$-$PbO_2$ by up to 0.09 Å occur depending on the method of preparation [40] and the maximum pressure reached in an experiment [4]. The same behaviour has also been observed for the $\alpha$-$PbO_2$-type phase of $TiO_2$ [41, 42]. It was also apparent that in the data for $\alpha$-$PbO_2$, while there was good agreement between the observed and calculated positions of most diffraction peaks, the observed 020 $d$-value was lower than the calculated value by up to 0.05 Å. This peak coincides with the strongest reflection from the remaining cotunnite phase; however, on recompression it was found to disappear at the II $\rightarrow$ III transition and then reappear upon decompression, shifted by the same amount as it had been in the first decompression cycle, indicating that the cotunnite-type phase might not have been retained down to ambient pressure in the first decompression run. Peak shifts and other anomalies have been reported previously [40] for $\alpha$-$PbO_2$ samples and attributed to lattice strain, loss of coherency and

probable cation disorder. In fact in one such sample, the intensity of the 020 reflection was almost zero, indicating a loss of coherency along [010].

### *3.6. Colour changes*

Under ambient conditions, rutile-type $\beta$-$PbO_2$ is black. Above 4 GPa, a colour change was observed in which the sample became red corresponding to the second-order I $\rightarrow$ I′ transition. Significant darkening was observed at the I′ $\rightarrow$ III transition, and at the III $\rightarrow$ IV transition the sample became transparent and remained red up to 47 GPa. These observations are in agreement with those of Liu [4]. Upon decompression, the sample turned black at 18.4 GPa and remained black through phases IV and III and down to ambient conditions in the $\alpha$-$PbO_2$ phase. Upon recompression of $\alpha$-$PbO_2$, the sample became red above 5.0 GPa.

Liu interpreted the first colour change on compression as being due to a transition between $\beta$-$PbO_2$ and $\alpha$-$PbO_2$. The present results indicate that the colour change occurs in $\beta$-$PbO_2$ near the I $\rightarrow$ I′ transition and in $\alpha$-$PbO_2$ in the absence of a transition. Upon removal of the gasket at ambient pressure, the material in the gasket hole was found to be black and a Debye–Scherrer pattern indicated that this material was $\alpha$-$PbO_2$. A small amount of red material was found on the gasket, for which a $\beta$-$PbO_2$ diffraction pattern was obtained yielding the following cell constants: $a = 4.9493(9)$ Å and $c = 3.3836(11)$ Å. These cell constants are both slightly smaller than those of the initial starting material due to the high stress experienced by this material. The colour change in $\beta$- and $\alpha$-$PbO_2$ could be due to a stress-induced opening in the band gap.

The darkening at the I′ $\rightarrow$ III transition indicates that the cubic phase has a more metallic character, whereas it is less metallic in phases IV and V.

### *3.7. Compressibility data and equations of state (EOS)*

The experimental data for the five phases of $PbO_2$ were fitted using a Birch–Murnaghan EOS [43]:

$$P = 1.5B_0[(V/V_0)^{-7/3} - (V/V_0)^{-5/3}][1 + 0.75(B_0' - 4)((V/V_0)^{-2/3} - 1)]$$

where $B_0$ is the bulk modulus at ambient pressure and $B_0'$ its first derivative with respect to pressure; see figure 2 and table 5. The data were also fitted using the H11 equation [44]; in this procedure $B_0'$ was calculated yielding values between 3.7 and 3.9 for $PbO_2$. The mean linear compressibilities are listed in table 3.

The $B_0$-values obtained for rutile-type $PbO_2$ are in agreement with the 170 GPa expected from bulk modulus–volume systematics [45]: $B_0 = 700S^2Z_AZ_C/V_0$, where $S$ is the ionicity ($S^2 = 0.5$ for oxides), $Z_A$ and $Z_C$ are the anion and cation charges, respectively and $V_0$ is the mean molar volume per ion pair in $cm^3$. $PbO_2$ as expected has the lowest bulk modulus of the rutile-type dioxides [46]. All of these dioxides are significantly more compressible along $\boldsymbol{a}$ than along $\boldsymbol{c}$. This arises from cation–cation and anion–anion repulsions in the $\boldsymbol{c}$-direction along which the chains of edge-sharing octahedra lie. A very slight decrease in $B_0$ is observed at the I $\rightarrow$ I′ transition as is expected at a second-order transition.

The bulk modulus of phase III (233 GPa), which was obtained by fitting the present data and the phase III data point of Yagi and Akimoto [3], is significantly higher than the 185 GPa expected from $B_0$–$V_0$ systematics. This is the case for most modified fluorite and fluorite-type oxides; for example the bulk moduli of $UO_2$, $CeO_2$ and $ThO_2$, with $V_0$-values *larger* than that of cubic $PbO_2$, range from 207 to 264 GPa [8, 11, 12, 47], and the $B_0$ of cubic $RuO_2$ is 399 GPa [20].

The bulk modulus of the orthorhombic phase IV (180 GPa) is lower than that of phase III; this can be attributed to the greater number of available mechanisms for compression in this lower-symmetry phase. Similar decreases in bulk modulus when going from a low-pressure to a related high-pressure structure have been documented for other systems in which there are additional compression mechanisms in the high-pressure phase. These transitions typically involve a reduction in symmetry. Examples include the pressure-induced transitions in cristobalite-$SiO_2$ [48], $TeO_2$ [49], $ReO_3$ [50], $BaBiO_3$ [51], $Na_{0.62}WO_3$ [52], $Mo_8O_{23}$ [53] and $RbTi_2(PO_4)_3$ [54]. The experimental $B_0$-value for $PbO_2$ phase IV is in good agreement with the 186 GPa predicted by systematics. The bulk modulus of the cotunnite-type $PbO_2$ (221 GPa) is to within experimental error equivalent to that of the cubic phase. There is greater uncertainty in this value along with that for phase IV as $V_0$ could not be measured directly, but had to be estimated by extrapolation. The value obtained for the cotunnite-type phase is much lower than the values reported for cotunnite-type $ZrO_2$ and $CeO_2$—332 and 304 GPa, respectively [14, 11]—but instead is in agreement with the 209 GPa predicted by systematics. The compression of the cotunnite-type phase was found to be anisotropic, with the $\boldsymbol{c}$-direction being the most compressible as is the case for $ZrO_2$ [14].

The bulk modulus of $\alpha$-$PbO_2$ (141 GPa) is less than that of rutile-type $\beta$-$PbO_2$ (176 GPa). This is identical to what was observed for the corresponding phases of $TiO_2$ [42]. Whereas the rutile and $\alpha$-$PbO_2$ both consist of edge-sharing octahedra, the way in which they are linked is different, with the former containing straight chains of octahedra and the latter zigzag chains. In addition, in the case of $\alpha$-$PbO_2$, the octahedra are themselves distorted with a minimum cation–cation distance of 3.456 Å as opposed to the distance of 3.3854 Å for phase I. The $\alpha$-$PbO_2$ structure hence has more possible mechanisms for compression. As in $\alpha$-$PbO_2$-type $TiO_2$, the $\boldsymbol{a}$-direction was found to be much less compressible than the other directions. It is along $\boldsymbol{a}$ that the shortest O–O contacts are found: 2.720 Å as opposed to the second-shortest O–O distances of 2.976 Å lying in the *yz* plane. The zigzag chains of edge-sharing octahedra are parallel to $\boldsymbol{c}$, the direction of intermediate compressibility. The longest polyhedral Pb–O distances of 2.227 Å are primarily directed along the highly compressible $\boldsymbol{b}$-direction.

### *3.8. The phase transition sequence in the rutile-type dioxides*

$PbO_2$ presents a model for the behaviour of the other rutile-type dioxides as this is the first example of a rutile-type dioxide undergoing a series of transitions and ultimately transforming to the cotunnite structure. This series of transitions

rutile $\rightarrow$ $CaCl_2$ $\rightarrow$ modified fluorite $\rightarrow$ orthorhombic $PbO_2$ phase IV $\rightarrow$ cotunnite

is of considerable importance for the other dioxides. The $CaCl_2$ phase and orthorhombic phase IV represent essential intermediate steps along this pathway. The distortion of rutile to $CaCl_2$ is the first step along a possible route to the $Pa\bar{3}$ structure involving a diffusionless displacement of the anions. The orthorhombic structure of phase IV is a distortion of the $Pa\bar{3}$ structure in which the cations are free to move for the first time in this sequence. This liberation of the cations is a preparation for the transition to the cotunnite structure, which requires significant modification to both the cation and anion sublattices.

Several dioxides with smaller cations undergo one or more steps along this pathway in the pressure range up to 50 GPa. $SiO_2$ [17, 18] and $MnO_2$ [19] undergo the the second-order transition to the $CaCl_2$-type structure, whereas the larger-cation dioxides $RuO_2$ [20] and $SnO_2$ [21] undergo the first two transitions. Calculations indicate that at 150 GPa,

$SiO_2$ will also transform to the $Pa\bar{3}$ structure [55]. This pathway therefore has important geophysical implications. The $\alpha$-$PbO_2$ phase is observed in addition for the oxides with the largest cations, $SnO_2$ and $PbO_2$. This phase is stabilized relative to rutile due to reduced cation–cation repulsive interactions. It should be noted that the group IVa (Ti, Zr, Hf) dioxides do not follow this pathway, but rather pass via a baddeleyite structure [56].

## 4. Summary

Up to 47 GPa, lead dioxide was found to undergo a series of four transitions beginning with the rutile structure and terminating with the cotunnite structure. A first transition to a metastable $CaCl_2$-type phase is observed at close to 4 GPa. At 7 GPa, $PbO_2$ transforms to the $Pa\bar{3}$ structure, corresponding to an increase in coordination number from 6 to 6+2. A further transition to an orthorhombic phase with $Z = 8$ occurs at 11.4 GPa. This phase could be isostructural to the orthorhombic I phase of $ZrO_2$ and that of $HfO_2$, in which the coordination number is 7. These cubic and orthorhombic phases were previously thought to be fluorite structured and tetragonally distorted fluorite structured, respectively. A final transition to the cotunnite structure (CN = 9) is observed beginning above 29 GPa. The transition to this structure is expected on the basis of ionic radius ratios. This transition pathway is of great importance for the other group IVb dioxides and has geophysical implications as the probable high-pressure structural sequence for stishovite.

## References

[1] White W B, Dachille F and Roy R 1961 *J. Am. Ceram. Soc.* **44** 170
[2] Syono Y and Akimoto S 1968 *Mater. Res. Bull.* **3** 153
[3] Yagi T and Akimoto S 1980 *J. Geophys. Res.* **85** 6991
[4] Liu L-G 1980 *Phys. Chem. Minerals* **6** 187
[5] Ming L C and Manghnani M H 1982 *High-Pressure Research in Geophysics* ed S Akimoto and M H Manghnani (Tokyo: Centre Academic)
p 329
[6] Haines J, Léger J M and Schulte O 1996 *Science* at press
[7] Liu L-G 1980 *J. Phys. Chem. Solids* **41** 331
[8] Benjamin T M, Zou G, Mao H K and Bell P M 1981 *Carnegie Inst. Yearbook* **80** 280
[9] Liu L-G 1980 *Earth Planet. Sci. Lett.* **49** 166
[10] Kourouklis G A, Jayaraman A and Espinosa G P 1988 *Phys. Rev.* B **37** 4250
[11] Duclos S J, Vohra Y K, Ruoff A L, Jayaraman A and Espinosa G P 1988 *Phys. Rev.* B **38** 7755
[12] Dancausse J-P, Gering E, Heathman S and Benedict U 1990 *High Pressure Res.* **2** 381
[13] Jayaraman A and Kourouklis G A 1991 *Pramana—J. Phys.* **36** 133
[14] Haines J, Léger J M and Atouf A 1995 *J. Am. Ceram. Soc.* **78** 445
[15] Mao H K, Bell P M, Shaner J W and Steinberg D J 1978 *J. Appl. Phys.* **49** 3276
[16] Rodríguez-Carvajal J 1990 *Satellite Meeting on Powder Diffraction (XVth Conf. of the International Union of Crystallography (Toulouse, France))* p 127
[17] Tsuchida Y and Yagi T 1989 *Nature* **340** 217
[18] Kingma K J, Cohen R E, Hemley R J and Mao H K 1995 *Nature* **374** 343
[19] Haines J, Léger J M and Hoyau S 1995 *J. Phys. Chem. Solids* **56** 965
[20] Haines J and Léger J M 1993 *Phys. Rev.* B **48** 13 344
[21] Haines J and Léger J M to be published
[22] Tang J T and Endo S 1993 *J. Am. Ceram. Soc* **76** 796
[23] Endo S, Nitawaki S, Shige T, Akahama Y, Kikegawa T and Shimomura O 1990 *High Pressure Res.* **4** 408
[24] Teufer G 1962 *Acta Crystallogr.* **15** 1187
[25] Curtis C E, Doney L M and Johnson J R 1954 *J. Am. Ceram. Soc* **37** 458
[26] Ohtaka O, Yamanaka T, Kume S, Hara N, Asano H and Izumi F 1990 *Proc. Japan Acad.* B **66** 193
[27] Ohtaka O, Yamanaka T and Kume S 1991 *Seramikkusu Kyokai Gakujutsu Ronbunshi* **99** 826
[28] Hamaya N 1994 private communication

[29] Yagi T, Jamieson J C and Moore P B 1979 *J. Geophys. Res.* **84** 1113
[30] Smolander K J 1982 *Phys. Scr.* **25** 425
[31] Kudoh Y, Takeda H and Arashi H 1986 *Phys. Chem. Minerals* **13** 233
[32] Sahl K and Zeeman J 1961 *Naturwissenschaften* **20** 641
[33] Beck H P 1979 *Z. Anorg. (Allg.) Chem.* **459** 81
[34] Léger J M, Haines J and Atouf A 1995 *Phys. Rev.* B **51** 3902
[35] Léger J M, Haines J and Atouf A 1995 *J. Appl. Crystallogr.* **28** 416
[36] Léger J M, Haines J and Atouf A 1996 *J. Phys. Chem. Solids* **57** 7
[37] Léger J M, Haines J, Atouf A, Schulte O and Hull S 1995 *Phys. Rev.* B **52** 13 247
[38] Block S, Da Jornada J A H and Piermarini G J 1985 *J. Am. Ceram. Soc.* **68** 497
[39] Kusaba K, Fukuoka K and Syono Y 1991 *J. Phys. Chem. Solids* **52** 845
[40] Hill R J 1982 *Mater. Res. Bull.* **17** 769
[41] Linde R K and DeCarli P S 1969 *J. Chem. Phys* **50** 319
[42] Haines J and Léger J M 1993 *Physica* B **192** 233
[43] Birch F 1952 *J. Geophys. Res.* **57** 227
[44] Holzapfel W B 1991 *Europhys. Lett.* **16** 67
[45] Anderson O L 1972 *The Nature of the Solid Earth* ed E C Robertson (New York: McGraw-Hill) p 575
[46] Hazen R M and Finger L W 1981 *J. Phys. Chem. Solids* **42** 143
[47] Gerward L, Staun Olsen J, Benedict U, Dancausse J-P, and Heathman S 1994 *High Pressure Science and Technology—1993* ed S L Schmidt, J W Shaner, G A Samara and M Ross (New York: AIP Press) p 453
[48] Palmer D C and Finger L W 1994 *Am. Mineral.* **79** 1
[49] Worlton T G and Beyerlein R A 1975 *Phys. Rev.* B **12** 1899
[50] Jørgensen J-E, Jorgensen J D, Batlogg B, Remeika J P and Axe J D 1986 *Phys. Rev.* B **33** 4793
[51] Sugiura H and Yamadaya T 1984 *Solid State Commun.* **49** 499
[52] Hazen R M and Finger L W 1984 *J. Appl. Phys.* **56** 311
[53] Sowa H, Steurer W and De Boer J L 1994 *Phase Transitions* **47** 1
[54] Hazen R M, Palmer D C, Finger L W, Stucky G D, Harrison W T A and Gier T E 1994 *J. Phys.: Condens. Matter* **6** 1333
[55] Cohen R E 1992 *High-Pressure Research: Application to Earth and Planetary Sciences* ed M H Manghnani and Y Syono (Washington, DC: Terra Scientific) p 425
[56] Sato H, Endo S, Sugiyama M, Kikegawa T, Shimomura O and Kusaba K 1991 *Science* **251** 786
[57] Cohen R E, Mehl M J and Boyer L L 1988 *Physica* B **150** 1